J. Fluid Mech. (1980), *vol.* 98, *part* 4, *pp.* 787–801
Printed in Great Britain

A mathematical model for fluid flow in a weld pool at high currents

By D. R. ATTHEY

Central Electricity Generating Board, Marchwood Engineering Laboratories, Southampton SO4 4ZB, England

(Received 9 January 1979 and in revised form 23 May 1979)

In order to determine the heat transfer inside a TIG (tungsten/inert gas) weld pool, it is necessary to have a good understanding of the flow patterns of the liquid metal. The principal force driving the fluid motion is the electromagnetic $\mathbf{j} \times \mathbf{B}$ force due to the current from the welding arc and its self-magnetic field. In this paper we consider the flow of a viscous incompressible conducting fluid in a hemispherical container due to various distributions of the electric current. The problem is posed as a time-dependent problem and is solved numerically using the Du Fort–Frankel leap-frog method. Results are presented for currents of 100 A flowing through the weld pool. This is a typical current for TIG welding, and corresponds to a Reynolds number in the range $200 < Re < 600$. Previous solutions of the problem were restricted to low Reynolds numbers, i.e. low currents.

1. Introduction

In recent years there has been a considerable amount of interest in understanding the physical mechanisms underlying welding processes. Most of this work has been towards understanding the TIG (tungsten/inert gas) welding process, where the source of heat is an electric arc and where no filler metal is added to the weld. An early attack on the problem was by Rosenthal (1941) who considered the heat flow due to a point source of heat traversing the surface of a semi-infinite block of material. The extensions of this work to cover plates of finite thickness or a distributed source of heat rather than a point source are straightforward numerical exercises. A more difficult extension of the Rosenthal work is to include the latent heat of fusion at the solid–liquid boundary. Longworth (1975) has developed a numerical method which takes account of the latent heat and allows the thermal properties to be functions of temperature.

All of the above techniques ignore any convective motions in the liquid. Recent experiments (Woods & Milner 1971; Kublanov & Erokhin 1974) have demonstrated that the weld pool produced by a TIG arc is vigorously stirred and that the stirring is driven primarily by electro-magnetic forces, the contribution due to thermal convection being very small by comparison. We may verify that the effects of thermal convection should be small by comparing the magnitude of the thermal and electromagnetic stirring forces. The ratio of these two forces is $g\Delta\rho/(\mu_0 I^2/\pi^2 a^3)$, where g, $\Delta\rho$, I, μ_0 and a are the acceleration due to gravity, the change in density, the total current, the permeability of the weld metal and the pool radius respectively. Inserting

0022–1120/80/4459–1210 $02.00 © 1980 Cambridge University Press

typical values of $\Delta\rho = 500\,\mathrm{kg\,m^{-3}}$ (which corresponds to a temperature difference of 600 °C in the pool), $I = 100$ A and $a = 2{\cdot}5$ mm, this ratio takes a value of 0·06.

We shall now estimate a value for the magnetic Reynolds number $R_m = \mu_0 \sigma a v_0$, where σ and v_0 are electrical conductivity of the weld metal and a typical flow velocity. Inserting typical values of $a = 2{\cdot}5$ mm and $v_0 = 50\,\mathrm{mm\,s^{-1}}$, we find that $R_m \sim 10^{-4}$. This confirms the result of Shercliff (1970) that the back e.m.f. generated by the metal flow is small. We shall therefore evaluate the electromagnetic stirring force corresponding to a stationary pool and use that throughout our calculations. The value of v_0 used above is a typical velocity predicted by the model in this paper and is shown by Woods & Milner (1971) to at least be of the correct order of magnitude.

Some theoretical attention has been directed towards the problem of weld pool stirring in the last few years. Shercliff (1970) considered the flow of a semi-infinite inviscid fluid due to a point source of current and showed that the solution possesses a singularity on the axis of symmetry. Sozou (1971) added viscosity to the model and showed that this removed the singularity unless a dimensionless parameter

$$K = \mu_0 I^2 / 2\pi^2 \rho \nu^2$$

exceeded a value of about 300. In this expression ρ and ν are the density of the material and the kinematic viscosity of the material. Inserting typical values for molten steel we find that the maximum current for which no singularities occur is around 4 A, which is much smaller than typical welding currents. The parameter K occurs naturally in the solution of the above semi-infinite problem, where it is impossible to form a length scale. We note that, for the flow in a finite container, the ratio of the electromagnetic forces to the viscous forces is $2\pi^2 K/Re$, where Re is the Reynolds number.

Sozou & Pickering (1976) found the solution for a point source of current acting at the centre of a finite hemisphere. For a free surface boundary condition on the top surface rather than a no-slip boundary condition, the critical value of K is reduced to about 94; above this value singularities will appear in the velocity field. They also tackled the problem numerically, and were unable to obtain a numerical solution above $K = 20$. Andrews & Craine (1978) looked at the problem of flow in a hemisphere with a distributed source of current. This is more realistic physically as the current from the arc typically enters the weld pool over a disc of radius about half the width of the pool. They were only able to treat the case of low-Reynolds-number flow, which is a valid approximation for low currents (up to 10 A passing through the weld pool). Unlike the point source cases, there was no indication of singularities in the velocity field. Andrews & Craine also found that the flow could rotate in either direction (i.e. either up or down the axis), depending on the nature of the current source, whereas the point source of current always produced a flow down the axis.

Sozou & Pickering (1978) have also considered the problem of fluid flow in an axisymmetric container of fluid when the current is produced by an electrode in contact with the liquid surface. They solved the problem for the case of a low Reynolds number. The boundary condition that they used (i.e. part of the upper pool surface in contact with an electrode) is relevant to the results of model experiments to study flow patterns in a low-melting-point material such as those performed by Kublanov & Erokhin (1974). However, in TIG welding the tip of the electrode is typically 3 mm above the pool surface and the current is transmitted to the pool via the ionized shielding gas and metal vapour in the arc. We have been unable to obtain an estimate

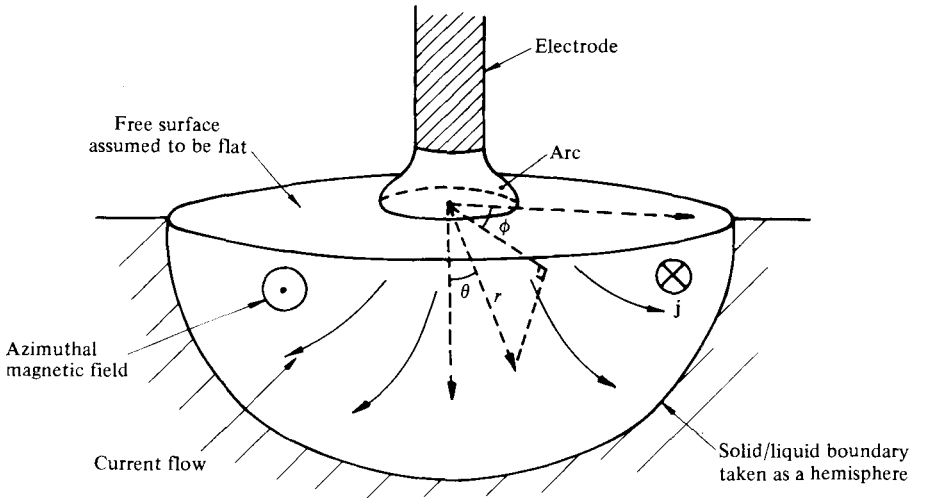

FIGURE 1. Schematic diagram of stirring process.

of the viscosity of this arc gas; however we would expect it to be much smaller than the viscosity of the liquid weld metal. We shall therefore model the TIG welding process by taking the upper pool surface as stress-free.

In this paper we shall consider the steady-state fluid flow in a hemispherical weld pool produced by a distributed source of current. Unlike Andrews & Craine we shall include the nonlinear terms in our treatment of the Navier–Stokes equations and we shall solve these equations numerically. This means that the results will predict the flow in a hemisphere for much higher currents than were possible with the linear model; indeed our solution will break down only when the laminar flow becomes unstable and the flow becomes turbulent. Our results indicate that this does not happen for currents of up to at least 100 A.

2. Formulation of the problem

The fluid flow in a weld pool must satisfy the Navier–Stokes equations

$$\nabla . \mathbf{v} = 0, \tag{1}$$

$$\partial \mathbf{v}/\partial t + (\mathbf{v} . \nabla)\, \mathbf{v} = -(1/\rho)\, \nabla p + (1/\rho)\, \mathbf{j} \times \mathbf{B} + \nu \nabla^2 \mathbf{v}, \tag{2}$$

together with appropriate boundary conditions, where $\mathbf{v}$, p, $\mathbf{j}$, and $\mathbf{B}$ refer to the fluid velocity, the pressure, the current density and the magnetic field respectively. Because of our assumptions of axial symmetry in the specification of the problem, we may expand equations (1) and (2) in spherical polar co-ordinates r, θ and ϕ, and set the ϕ derivatives equal to zero. The co-ordinate system is shown in figure 1.

In recent years a large number of numerical methods have been developed for the solution of the Navier–Stokes equations, and a comprehensive survey is given by Roache (1972). The method we shall use determines the solution of the unsteady Navier–Stokes equations from some initial solution, e.g. $\mathbf{v} = 0$. At first sight it would appear to be an unnecessary complication to determine the solution to a steady-state elliptic problem by adding a time derivative and solving the resulting parabolic

problem. However, it is shown in Roache that the solution of the initial-value problem by a step-by-step method is equivalent to the solution of the original steady-state problem by the iterative technique of relaxation.

We note that the use of a Stokes stream function ψ will ensure that the continuity equation (1) is satisfied. Accordingly we set

$$\mathbf{v} = \nabla \times (0, 0, \psi/r \sin\theta). \tag{3}$$

It will prove convenient to set

$$\omega = \nabla \times \mathbf{v} = (0, 0, Q/r \sin\theta). \tag{4}$$

We now introduce dimensionless variables. We put

$$R = r/a, \quad \tau = \nu t/a^2, \quad \mathbf{F} = (4\pi^2 a^4/\mu_0 I^2) \nabla \times (\mathbf{j} \times \mathbf{B}),$$
$$\Psi = 2\psi/a\nu, \quad \mathbf{V} = 2a\mathbf{v}/\nu \quad \text{and} \quad \Omega = 2aQ/\nu. \tag{5}$$

Taking the curl of equation (2), we obtain

$$\partial\Omega/\partial\tau + \tfrac{1}{2}R \sin\theta \{\nabla' \times (\mathbf{V} \cdot \nabla') \mathbf{V}\}_\phi = KFR \sin\theta + D\Omega, \tag{6}$$

where ∇' is the dimensionless vector differential operator, F is the ϕ component of the vector $\mathbf{F}$ and the operator D is defined by

$$D = \{\partial^2/\partial R^2 + (1/R^2)(\partial^2/\partial\theta^2 - \cot\theta\, \partial/\partial\theta)\}. \tag{7}$$

Combining equations (3) and (4) gives

$$D\Psi = -\Omega. \tag{8}$$

Equation (6) is not the most convenient form for the momentum equation. We may expand the nonlinear advection term in (6) to give

$$\partial\Omega/\partial\tau + \tfrac{1}{2}R^2 \sin^2\theta \nabla' \cdot (\mathbf{V}\Omega/R^2 \sin^2\theta) = KFR \sin\theta + D\Omega, \tag{9}$$

which is equivalent to

$$\partial\xi/\partial\tau + \tfrac{1}{2}\nabla' \cdot (\mathbf{V}\xi) = \ldots,$$

where $\xi = \Omega/R^2 \sin^2\theta$, and hence it is a conservation equation. It has been shown that it is generally advantageous to formulate fluid flow equations in conservation form. By doing so and taking central differences we ensure that the finite-difference scheme also possesses the conservation property. It has been found that conservative difference schemes are generally more accurate than non-conservative schemes, although the truncation errors are of the same order (Roache 1972).

Equations (8) and (9) must be solved subject to suitable boundary conditions and initial conditions. The situation we wish to solve is that of flow in a hemisphere (see figure 1). We shall approximate the free surface between the liquid and vapour as being flat. The result of this approximation is that we are no longer able to prescribe the pressure on this surface, and it is possible that the pressure will be significantly different from atmospheric. The validity of our approximation will be considered in § 5.

The boundary conditions that are required are that both Ψ and Ω should be specified at all points on the boundary of the region of interest, i.e. on $R = 0$, $R = 1$, $\theta = 0$ and $\theta = \frac{1}{2}\pi$. As there is no normal component of flow across the boundary, we have as one condition

$$\Psi = 0 \tag{10}$$

at all points on the boundary. The second boundary condition will be different for different segments of the boundary. On the 'free surface' $\theta = \frac{1}{2}\pi$ we require the tangential component of stress to be continuous. We noted in the introduction that the viscosity of the arc gas is small by comparison with that of the liquid, so we impose the condition that the tangential shear stress is zero in the liquid. This is equivalent to the condition that the vorticity is zero, i.e.

$$\Omega = 0 \quad \text{on} \quad \theta = \tfrac{1}{2}\pi. \tag{11}$$

On the axis, $\theta = 0$ the condition of symmetry again shows that the vorticity must be zero, i.e.

$$\lim_{\theta \to 0} \Omega/\sin\theta = 0. \tag{12}$$

Since the corner $R = 0$ is a stagnation point we expect the vorticity to be single-valued there, so $\Omega/R \sin\theta \to 0$ as we approach the corner from any direction, i.e.

$$\lim_{R \to 0} \Omega/R = 0. \tag{13}$$

Finally on the outer boundary, $R = 1$, the tangential component of velocity must be zero as well as the normal component, so

$$\partial\Psi/\partial R = 0 \quad \text{on} \quad R = 1. \tag{14}$$

To complete the specification of the problem we need two initial conditions. The simplest are

$$\Psi = \Omega = 0 \quad \text{for} \quad \tau = 0. \tag{15}$$

Other initial conditions that can be used are

$$\Psi = \Psi_0, \quad \Omega = \Omega_0 \quad \text{for} \quad \tau = 0, \tag{16}$$

where Ψ_0 and Ω_0 are the solution to a flow problem with a current distribution similar to that being considered. As we are only interested in the steady-state solution to the Navier–Stokes equations, our final solution should be independent of the choice of initial conditions. The choice of initial condition might be expected to alter the time taken for the transient effects to decay, and thus reduce the computation time. This point will be discussed further in a later section.

3. Numerical solution of the Navier–Stokes equations

3.1. *Finite-difference equations*

We first divide up the region of interest using a finite-difference mesh. To do this, we choose integers J and K and set $\delta R = 1/(J-1)$, $\delta\theta = \pi/2(K-1)$. We also choose a time step $\delta\tau$ and we use the notation $\Psi^n_{j,k}$ to represent the value of Ψ at the (j,k)th grid point and the nth timestep, i.e.

$$\Psi^n_{j,k} = \Psi\{(j-1)\,\delta R, (k-1)\,\delta\theta, n\,\delta\tau\}, \tag{17}$$

with a similar notation for Ω. We also set

$$\begin{aligned} R_j &= (j-1)\,\delta R, \quad \theta_k = (k-1)\,\delta\theta, \\ s_k &= \sin\theta_k \quad \text{and} \quad F_{j,k} = F(R_j, \theta_k). \end{aligned} \tag{18}$$

We shall solve the momentum equation using the Du Fort–Frankel leap-frog method. This method approximates the differential equation by an explicit finite-difference scheme using three time levels. The vorticity variable Ω is only evaluated at alternate mesh points at any time level. For details of the method we refer to Moore, Peckover & Weiss (1973) and Weir (1976).

Taking central differences of equation (9) and rearranging gives

$$\begin{aligned}\Omega_{j,k}^{n+1} = \Omega_{j,k}^{n-1} &+ \{2\delta\tau/(R_j^2\,\delta\theta^2 + \delta\tau(s_k/s_{k+\frac{1}{2}} + s_k/s_{k-\frac{1}{2}} + 2R_j^2\,\delta\theta^2/\delta R^2))\}\\ &\times \{A_{j,k}^n R_j^2\,\delta\theta^2 + KF_{j,k} R_j^3 s_k\,\delta\theta^2 + (\Omega_{j+1,k}^n - 2\Omega_{j,k}^{n-1} + \Omega_{j-1,k}^n)\\ &\times R_j^2\,\delta\theta^2/\delta R^2 + s_k((\Omega_{j,k+1}^n - \Omega_{j,k}^{n-1})/s_{k+\frac{1}{2}} + (\Omega_{j,k-1}^n - \Omega_{j,k}^{n-1})/s_{k-\frac{1}{2}})\},\end{aligned} \tag{19}$$

where the $A_{j,k}^n$ refers to the advection term, i.e.

$$\begin{aligned}A_{j,k}^n = &-\tfrac{1}{2}\{(\Omega_{j+1,k}/R_{j+1}^2 s_k)(\Psi_{j+1,k+1} - \Psi_{j+1,k-1})\\ &-(\Omega_{j-1,k}/R_{j-1}^2 s_k)(\Psi_{j-1,k+1} - \Psi_{j-1,k-1})\}/4\delta R\,\delta\theta\\ &+\tfrac{1}{2}(s_k/R_j)\{(\Omega_{j,k+1}/R_j s_{k+1}^2)(\Psi_{j+1,k+1} - \Psi_{j-1,k+1})\\ &-(\Omega_{j,k-1}/R_j s_{k-1}^2)(\Psi_{j+1,k-1} - \Psi_{j-1,k-1})\}/4\delta R\,\delta\theta,\end{aligned} \tag{20}$$

all terms on the right-hand side of equation (20) being evaluated at time level n.

Once we have used the momentum equation to determine values of Ω on half the grid points at the new time level $(n+1)$, we use equation (8) relating the stream function and vorticity to determine the values of Ψ at the new time level. To obtain a useful scheme, we must approximate the operator D using only the values of Ψ on alternate grid points. By use of Taylor's theorem, we may show that equation (8) may be approximated by

$$\begin{aligned}-\Omega_{j,k} = &\{\Psi_{j+1,k+1} + \Psi_{j-1,k+1} + \Psi_{j+1,k-1} + \Psi_{j-1,k-1} - \tfrac{1}{2}(\Psi_{j+2,k} + \Psi_{j-2,k})\\ &-3\Psi_{j,k}\}/2R_j^2\,\delta\theta^2 + \{\Psi_{j+2,k} + \Psi_{j-2,k} - 2\Psi_{j,k}\}/4\delta R^2\\ &+\cot\theta_k\{\Psi_{j+1,k-1} + \Psi_{j-1,k-1} - \Psi_{j+1,k+1} - \Psi_{j-1,k+1}\}/4R_j^2\,\delta\theta,\end{aligned} \tag{21}$$

where all the values are at time $(n+1)$. The set of equations (21), together with boundary conditions which will be discussed in the next section, form a complete system of equations for the unknown $\Psi_{j,k}$ over half the grid points and may be solved by a relaxation method.

Unfortunately the values of Ψ produced by (21) are those on the wrong half of the grid to be able to advance the momentum equation by another time step. To advance the momentum equation we must first interpolate among the values of Ψ to determine the missing values. The most satisfactory interpolation procedure follows by noting that Ψ satisfies equation (8). If we use the usual five-point representation for the differential operator D and rearrange, we obtain

$$\begin{aligned}\Psi_{j,k} = &\{R_j^2\,\delta\theta^2(\Psi_{j+1,k} + \Psi_{j-1,k}) + \delta R^2(\Psi_{j,k+1} + \Psi_{j,k-1})\\ &-\tfrac{1}{2}\delta\theta\,\delta R^2\cot\theta_k(\Psi_{j,k+1} - \Psi_{j,k-1}) + R_j^2\,\delta\theta^2\delta R^2\Omega_{j,k}\}/2(R_j^2\,\delta\theta^2 + \delta R^2).\end{aligned} \tag{22}$$

In equation (22), all the terms are evaluated at time $(n+1)$. The value of Ψ on the left-hand side is that which we wish to determine, while the values on the right-hand side are known. The value of Ω on the right-hand side is not known; however it may simply be replaced by an average of values at surrounding points.

We have now evaluated all the relevant variables at time $(n+1)$ and we may proceed to time $(n+2)$ by exactly the same process. We proceed in this manner until successive values of both Ψ and Ω agree to within some desired accuracy at all points on the mesh.

3.2. *Boundary conditions*

We consider first the momentum equation. One difficulty in the boundary conditions is the representation of the no-slip boundary condition on the solid–liquid boundary. Orzag & Israeli (1974) discuss this problem and show that a balance must be struck between truncation error and stability in the choice of representation. Following their recommendation, we use a simple representation for the boundary condition, i.e.

$$\Omega_{j,k} = -2\Psi_{J-1,k}/\delta R^2. \tag{23}$$

The remaining boundary conditions for the momentum equation are applied in a straightforward manner.

We now consider the stream-function equation. The boundary condition $\Psi = 0$ does not give rise to any difficulty; the only problem is that for $j = 2$ and $J-1$ the seven-point formula (21) contains one non-existent point with $j = 0$ or $J+1$. Clearly we must rewrite the expression

$$\partial^2\Psi/\partial R^2 \simeq \{\Psi_{j+2,k} + \Psi_{j-2,k} - 2\Psi_{j,k}\}/4\delta R^2 \tag{24}$$

for $j = 2$ and $J-1$. Weir used a different seven-point formula close to the boundaries with (24) replaced by an expression for $\partial^2\Psi/\partial\theta^2$ with step length $2\delta\theta$. However, this approach will break down at the corners of the region, where yet another treatment is needed. An alternative strategy is to use Taylor's theorem and the two boundary conditions

$$\Psi = \partial\Psi/\partial R = 0 \quad \text{for} \quad R = 0$$

to obtain

$$\partial^2\Psi/\partial R^2 \simeq 2\Psi_{4,k}/9\delta R^2 \tag{25}$$

to the same accuracy as the rest of the scheme. A similar expression holds close to the outer boundary.

The initial conditions $\Psi = \Omega = 0$ were most frequently used. However, for some high-current flows it was found to reduce the computing time to take the initial conditions as the steady-state solution to a similar problem.

4. Expressions for the stirring force

We first consider the form for the stirring force F used by Andrews & Craine (1978). They evaluated the current distribution produced by a point source a distance b above the weld pool, and a point sink a distance c below the pool, with a constant value for the electrical conductivity everywhere. This produced an expression for the stirring force inside the weld pool as

$$F = (R_1^{-3} - R_2^{-3})\{2 - (b + R\cos\theta/R_1) - (c - R\cos\theta/R_2)\}/2R\sin\theta, \tag{26}$$

where R_1 and R_2 are the distances from the point (R, θ) to the source and the sink respectively, all distances being scaled by the pool radius, a.

With this form for the current distribution the velocity field is rather sensitive to the values of b and c. Unfortunately it is difficult to relate the values of b and c to any

experimental conditions. An added complication is that, with the above form for the stirring force, most of the current misses the pool altogether; for a typical case $b = c = 2$ only 11 % of the current passes through the weld pool, which is clearly unrealistic. Experimental results show that the current distribution is certainly more concentrated than this, although it is not clear just how concentrated it actually is. The maximum radius of the arc is typically around 4 mm, but it is believed that, at the plate, the current is focused so as to flow through an anode spot which is smaller than this (Quigley 1977).

Accordingly we shall consider an alternative formulation for the stirring-force problem. However, the form given by equation (26) and the corresponding solution of the linearized fluid flow problem will provide a useful check for our numerical scheme.

We now consider the current flow in a plate of finite thickness, g, due to a specified current input across the surface which coincides with the top of the pool. It is most convenient to tackle this problem in terms of cylindrical polar co-ordinates, so we set

$$u = r\sin\theta, \quad z = r\cos\theta. \tag{27}$$

We shall consider a particular form for the axial current flow across the upper surface of the plate

$$j_z = I\, e^{-u^2/u_0^2}/\pi u_0^2 \quad \text{on} \quad z = 0, \tag{28}$$

while assuming that the lower surface is electrically insulated gives

$$j_z = 0 \quad \text{on} \quad z = g. \tag{29}$$

Unfortunately it is not appropriate to solve this problem in terms of an electric potential η since η would have a logarithmic singularity as $u \to \infty$. Instead we may differentiate Laplace's equation for the potential and the boundary conditions (28) and (29) to formulate a problem for the radial current flow, j_u. This problem may be solved using a Hankel transform to give

$$j_u = (I/2\pi)\int_0^\infty s J_1(us)\, e^{-s^2u_0^2/4}\cosh s(g-z)\, ds/\sinh gs. \tag{30}$$

The expression for the axial current flow j_z is similar.

We may now integrate the equation

$$\mu_0 \mathbf{j} = \nabla \times \mathbf{B}$$

to determine the non-zero component of the magnetic field as

$$B_\phi = (\mu_0 I/2\pi)\int_0^\infty J_1(us)\, e^{-s^2u_0^2/4}\sinh s(g-z)\, ds/\sinh gs. \tag{31}$$

The expressions (30) and (31) may be evaluated numerically by a Gauss–Laguerre quadrature method. Finally, we may evaluate the stirring force as

$$F = 8\pi^2 a^4 j_u B_\phi/\mu_0 I^2 u. \tag{32}$$

5. Stability and accuracy

In order that the advective terms in the momentum equation should not lead to instabilities, we require that the Courant–Friedrich–Lewy conditions be satisfied, i.e. that

$$V_R\, \delta\tau/\delta R < 1 \tag{33}$$

and

$$V_\theta\, \delta\tau/R\delta\theta < 1. \tag{34}$$

The Du–Fort–Frankel representation of the diffusive term is always stable; however in order that it should be reasonably accurate we prefer

$$\delta\tau/\delta R^2 < \tfrac{1}{2}. \tag{35}$$

Accordingly the time step is initially chosen so as to satisfy condition (35) and subsequently it is modified if necessary to ensure that (33) and (34) are always satisfied.

In the numerical scheme there are several parameters which govern the accuracy by which two successive values of a variable must agree before we assume that an iterative scheme has converged. The three principal parameters govern the convergence of Ψ at each time step and the amount by which Ψ and Ω must agree at successive time steps for the steady-state solution to have been achieved. For most of the results quoted, these parameters have been taken as 10^{-4}. As a check that this was sufficiently small, a typical case was repeated with the parameters reduced to 5×10^{-5}. The resulting change in Ψ was no more than 0·5 %.

Most of the results quoted below were obtained with a 16×16 mesh, i.e. $\delta R = 1/15$, $\delta\theta = \pi/30$, or a 21×21 mesh. As a check on accuracy, a small number of cases were run with meshes of size 11×11 or 31×31. Comparison of the results indicated that the results quoted are accurate to within about 3 %.

A final possible source of error lies in the fact that we have taken the top surface of the pool to be flat. This means that we are unable to prescribe the normal stress on the top surface, and it is possible that there will be a significant discontinuity in pressure across this surface. In practice this discontinuity will be accounted for by a distortion in the top surface which will introduce variations in hydrostatic and surface tension pressures.

For convenience we shall estimate the effect of this pressure distribution in terms of dimensional variables. At the free surface the normal hydrodynamic stress

$$-p + (2\nu\rho/r)(v_r + \partial v_\theta/\partial\theta) \tag{36}$$

must be balanced by the surface tension of a suitably deformed surface. To determine the pressure p accurately is extremely difficult (Roache 1972); however it is simple enough to obtain a rough estimate of the pressure variation across the top surface by integrating the r component of the steady-state momentum equation across the upper surface to give

$$p + \tfrac{1}{2}\rho v_r^2 = -\int_r^a j_n B_\phi \, dr + \nu\rho \int_r^a (1/r^2)\, \partial Q/\partial\theta \, dr, \tag{37}$$

where we have taken the pressure to be zero at the edge of the pool surface, $r = a$. Taking the form (28) for the current input on the upper surface, the electromagnetic stirring force may be evaluated as

$$\int_r^a j_n B_\phi \, dr = \mu_0 I^2/(4\pi^2 u_0^2)\{-E_1(a^2/u_0^2) + E_1(2a^2/u_0^2) + E_1(r^2/u_0^2) - E_1(2r^2/u_0^2)\},$$

where $E_1(x)$ denotes the exponential integral (Abramowitz & Stegun 1964). Taking $I = 100\,\mathrm{A}$, $a = 2{\cdot}5\,\mathrm{mm}$ and $u_0 = 3\,\mathrm{mm}$, the electromagnetic term has a maximum value of around $15\,\mathrm{N\,m^{-2}}$, and each of the other terms in (36) and (37) takes value around $1\,\mathrm{N\,m^{-2}}$. As the surface tension of the pool surface should be no less than $1\,\mathrm{N\,m^{-1}}$, the stress difference may be accommodated by the pool surface having a

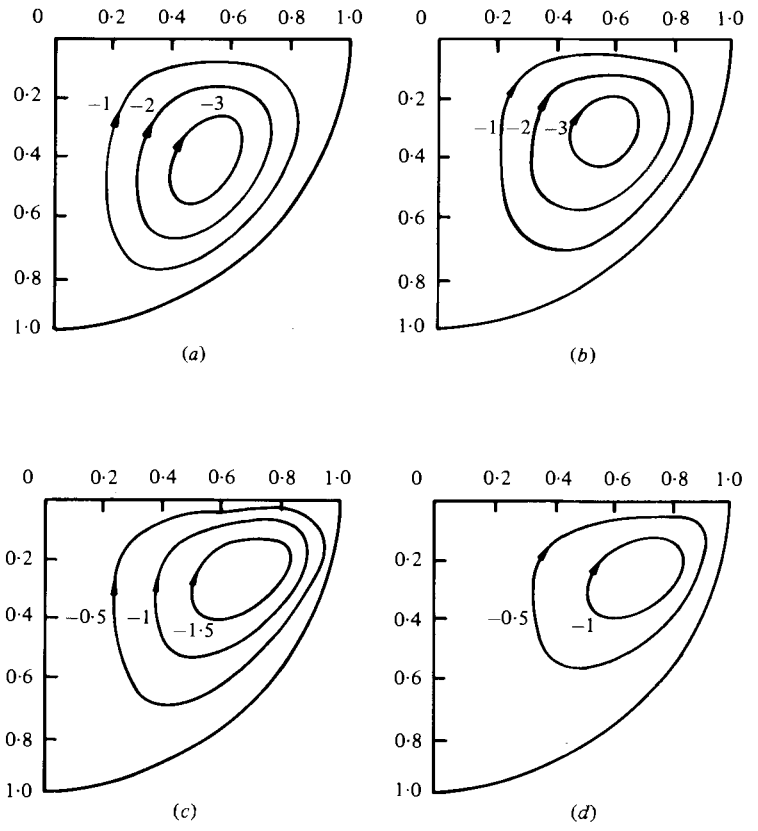

FIGURE 2. Dimensionless stream function $10^6\Psi/K$ for a point source and a point sink with $b/c = 1$. (*a*) $K = 8{\cdot}2$, (*b*) $K = 2{\cdot}0 \times 10^6$, (*c*) $K = 2{\cdot}3 \times 10^7$, (*d*) $K = 7{\cdot}3 \times 10^7$.

radius of curvature of 100 mm, and the pool surface may be taken as being flat to a good approximation. Taking a more concentrated current input with $u_0 = 1{\cdot}25$ mm, the maximum stress difference is around 160 N m^{-2} with the greatest contribution again coming from the electromagnetic term. This may be accommodated by a pool surface of radius of curvature 12 mm and it is just about acceptable to approximate the upper pool surface as being flat. For smaller values of u_0 this approximation would become invalid and consequently no results are presented for these cases.

6. Results

We consider first the current distribution used by Andrews & Craine with the current produced by a point source and a point sink. Figure 2 shows the streamlines for the case with a point source and a point sink each a distance $R = 2$ from the pool centre. The cases considered are $K = 8{\cdot}2$, $2{\cdot}0 \times 10^6$, $2{\cdot}3 \times 10^7$ and $7{\cdot}3 \times 10^7$, which correspond to $I = 0{\cdot}6$, 300, 1000 and 1800 A; however we note that only about $0{\cdot}11\,I$ actually passes through the weld pool. The case $I = 300$ shows only a small change from the linear (i.e. small-I) solution. Increasing I still further, the nonlinear terms in the equation begin to have a significant effect and the contours of Ψ are pushed towards the corner $\theta = \frac{1}{2}\pi$, $R = 1$. The values of Ψ increase with increasing K (or I).

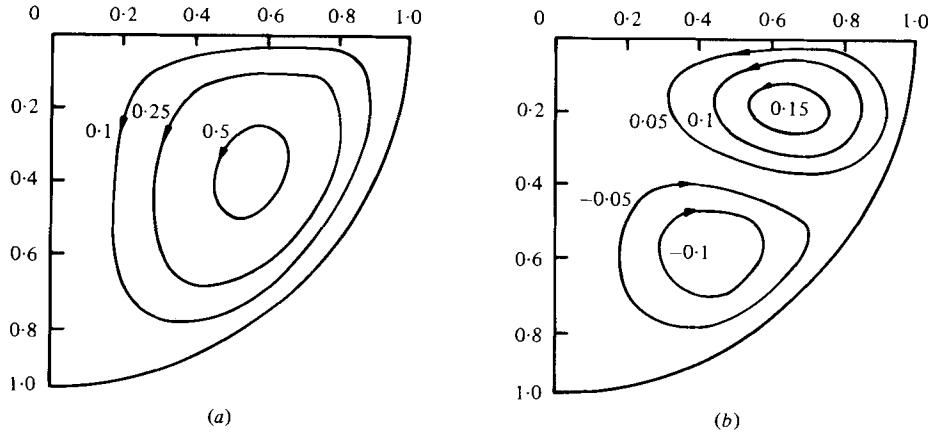

FIGURE 3. Dimensionless stream function $10^6\Psi/K$ for a point source and point sink with $K = 2{\cdot}3 \times 10^7$ ($I = 100$ A). (*a*) $b/c = 0{\cdot}5$, (*b*) $b/c = 0{\cdot}74$.

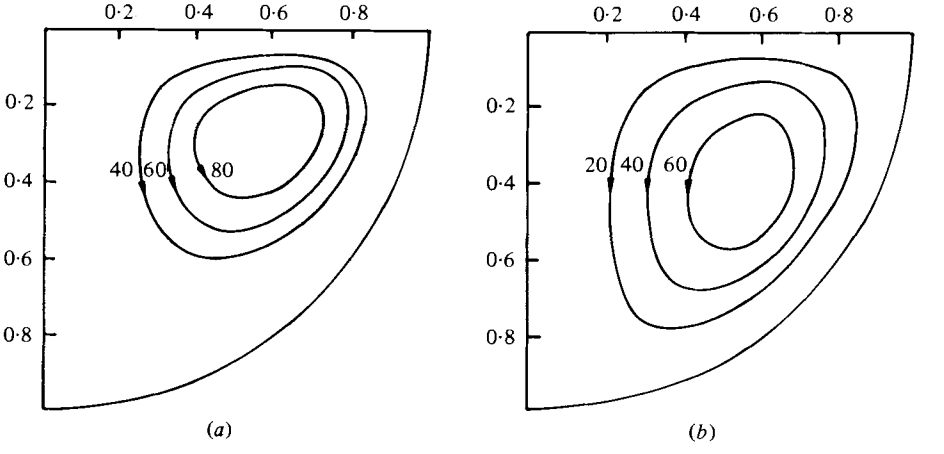

FIGURE 4. Dimensionless stream function $10^6\Psi/K$ for a Gaussian current input with decay radius $1{\cdot}2a$. (*a*) $I = 0{\cdot}1$ A, (*b*) $I = 100$ A.

For small K when the linear solution is valid, Ψ varies linearly with K. For larger values of K the increase is slightly slower than this; for $K = 7{\cdot}3 \times 10^7$ the maximum value of Ψ is about one-third of the value that would be obtained by scaling the linear solution. In all these cases Ψ is negative throughout the pool; i.e. the flow is up the axis of symmetry.

Andrews & Craine showed that by varying the positions of the source and the sink it was possible to change the direction of flow in the small-current case, or to produce two separate loops, one flowing clockwise and the other anticlockwise. Figure 3 shows that this behaviour is repeated for high currents, with $I = 1000$ A, although the streamlines have again been pushed outwards.

Figure 4 is a contour plot of the stream function Ψ using the Hankel transform method for generating the stirring force $\mathbf{j} \times \mathbf{B}$. The weld pool just penetrates the plate; i.e. the lower surface of the plate is a tangent plane to the hemisphere. The results are for small current (0·1 A) and a larger current (100 A). Figure 4 has the current density

	K					
	23	$2{\cdot}3\times10^3$	$2{\cdot}3\times10^5$	$2{\cdot}3\times10^5$	$2{\cdot}3\times10^5$	$2{\cdot}3\times10^5$
	u_0					
	0·8	0·8	0·8	1·2	0·6	0·5
$R = 0{\cdot}1$	0·101	9·67	2·24, 2	9·25, 1	4·44, 2	6·15, 2
0·2	0·127	12·75	3·51, 2	1·48, 2	6·27, 2	8·31, 2
0·3	0·135	14·08	4·41, 2	1·88, 2	7·80, 2	1·03, 3
0·4	0·125	13·58	4·88, 2	2·08, 2	8·45, 2	1·09, 3
0·5	0·101	11·50	4·93, 2	2·10, 2	8·67, 2	1·14, 3
0·6	0·072	8·50	4·57, 2	1·93, 2	8·13, 2	1·11, 3
0·7	0·043	5·25	3·86, 2	1·59, 2	7·51, 2	1·02, 3
0·8	0·020	2·50	2·83, 2	1·09, 2	5·87, 2	8·22, 2
0·9	0·005	0·64	1·41, 2	4·38, 1	3·88, 2	5·82, 2

TABLE 1. Dimensionless values of the axial velocity for the case where the lower plate surface is a tangent plane to the pool.

distribution on the top surface as a Gaussian which decays to $1/e$ of its maximum value in a distance $1{\cdot}2a$, where a is the weld pool radius. As we might expect the increasing current again causes the contours to move outwards and the dimensionless values of Ψ to decrease.

We also note that, when compared with the results of the analytic current distribution, the dimensionless values of the stream function are increased by a factor of about 100. This is because the stream function is divided by I^2 to produce the dimensionless stream function. For the Hankel transform current distributions most of the current I flows through the weld pool, whereas for the analytic distributions the current flowing through the weld pool is typically $0{\cdot}1\,I$.

Table 1 shows the variation of the axial velocity distribution with current and with the concentration of the current input. The values are given in floating-point form; i.e. y, n corresponds to $y\times10^n$. In addition to the above trends, we note that the magnitude of the axial velocity is strongly dependent on the nature of the current source. Reducing the decay radius of the current input considerably increases the axial velocity (and indeed the magnitude of the entire velocity distribution).

Figure 5 shows results for the same current input as in figure 4, the difference being that the weld pool in figure 5 does not fully penetrate the plate. The results are for the case where the plate thickness is twice the weld pool radius. In this case the current has a larger volume of metal to diverge into and consequently the stirring force, i.e. the rotational part of $\mathbf{j}\times\mathbf{B}$, and the fluid velocity are somewhat smaller. However, for an infinitely thick plate, electromagnetic stirring will still cause fluid flow in the pool. If we were to compute the flow for a plate of thickness greater than $2a$, the velocity would decrease with increasing plate thickness, approaching the velocity associated with a semi-infinite region in the limit. With a current distribution of decay radius $0{\cdot}8a$, the stream-function maps for plates of thickness a and $2a$ are very similar. This suggests that, for this fairly concentrated current input, the fluid flow for a plate of thickness a is already close to that for a semi-infinite region, so that increasing the plate thickness will have little effect on the flow.

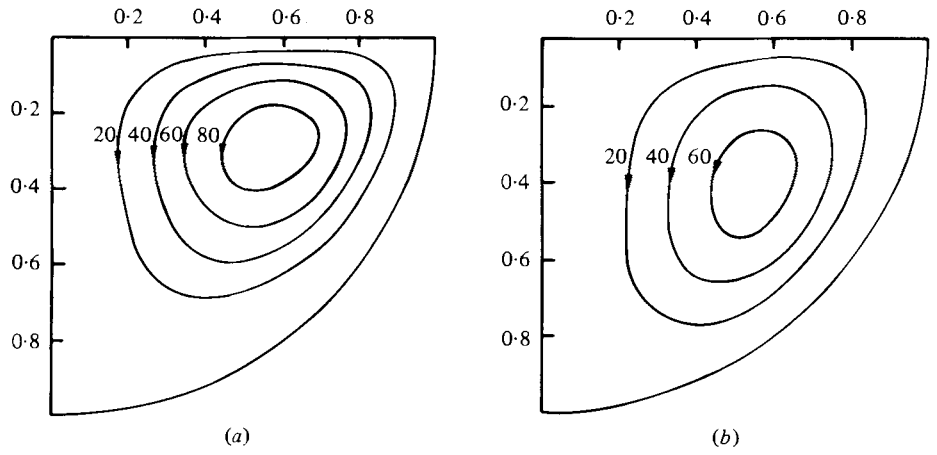

FIGURE 5. Dimensionless stream function $10^6\Psi/K$ for a Gaussian current input with decay radius $1{\cdot}2a$ in plate thickness $2a$. (*a*) $I = 0{\cdot}1$ A, (*b*) $I = 100$ A.

Finally we note that for a pool of 2·5 mm radius fully penetrating a plate with current distributions of decay radii 3, 2 and 1·5 mm, the maximum velocities on the axis of symmetry are 25 mm s^{-1}, 62 mm s^{-1} and 105 mm s^{-1} respectively.

7. Discussion

A question which has been the subject of some speculation in the past is whether the flow in the pool is laminar or turbulent. The only convincing way to answer this point would be by a stability analysis, which would be extremely difficult. The model used in this paper assumes that the flow is laminar and the results obtained are consistent with this assumption. However, as Roache (1972) points out, the critical Reynolds number above which the flow becomes turbulent can be either reduced or increased by effects of 'numerical diffusion', and consequently the numerical results do no more than suggest that the flow should be laminar. This suggestion is reinforced when we examine the Reynolds number of the flow. This satisfies $Re < 600$ for all the cases considered with $I = 100$ A and, although we do not know the critical Reynolds number for this problem, the critical Reynolds numbers for other interior flow problems are typically somewhat larger than 600 (Landau & Lifshitz 1959).

Unfortunately it does not appear to be possible to compare the results from this model with any experimental results. Woods & Milner (1971) conducted several experiments in hemispherical bowls, but they did not attempt to measure the velocity in these cases; instead they looked at the degree of mixing of various tracer materials. They did produce quantitative results for a model experiment with mercury in a rectangular bath, by measuring the velocity on the surface photographically. Because of the differences in geometry it is unreasonable to expect good agreement with their results; however it is encouraging that their observed maximum surface velocities of 25–80 mm s^{-1} for a current of 100 A are roughly similar to those predicted by our model.

Kublanov & Erokhin (1974) considered a model experiment with liquid gallium in a container which was a parabola of revolution. The maximum radius of the container was 50 mm and the velocities were in the range 50–100 mm s^{-1}. Kublanov & Erokhin

noted that the flow was turbulent, which is not surprising as the Reynolds number was around 10^4. It would be interesting to see what our laminar flow model would make of a situation where the physical flow is known to be turbulent; unfortunately this is not possible, as the stability restrictions (33) and (34) make $\delta\tau$ prohibitively small.

From equation (6) we see that the only parameter governing the magnitude of the dimensionless quantities $\mathbf{V}$ and Ω is Sozou's constant, K; the function F depends only on ratios of lengths (i.e. u_0/a for the Gaussian current input or b and c for the point source, point sink model) and, provided these ratios are kept constant, F will be independent of I and a. If V_0 is the typical magnitude of $\mathbf{V}$ for a particular flow, the Reynolds number is just $Re = \frac{1}{2}V_0$. This shows that for a model experiment in which the length scale is different from that of a weld pool it is important to keep the value of K the same. For example, to compare a TIG weld pool in steel using a current of 100 A with a model experiment in gallium, the model experiment should use a current of 45 A whatever the size of the container. The experiments of Kublanov & Erokhin used currents of 550–700 A and can only be compared with currents of over 1000 A in steel, i.e. currents much larger than those normally used in TIG welding.

We note that the direction of flow is down the axis for all the current distributions considered except one or two of the more artificial ones. Shercliff (1970) suggested that as long as j_u is positive throughout the pool (where u denotes the radial direction in cylindrical polar co-ordinates) then the flow will always be directed down the axis. For all the numerical current distributions considered in this paper j_u is indeed positive throughout the pool. Any physical situation where j_u is negative in the pool is probably of no practical significance to welding. The analytic current distributions which produced flow up the axis can therefore be dismissed as interesting but unrealistic.

Finally we may evaluate the Péclet number of the flow. For currents of 100 A the Péclet number lies in the range $10 < Pe < 70$ so that convection must be the dominant effect. As the fluid flow is down the axis, this means that the heat transfer is preferentially down the axis. The pool boundary is not necessarily hemispherical in practice; it is of course the surface on which the temperature is equal to the melting temperature. If the heating was from a point source in a thick block of metal and there was no fluid motion, the pool boundary would be hemispherical. The effect of the fluid flow is to deepen the pool; however the effect of the heat source being distributed over the surface of the pool is to make the pool shallower. To determine the shape of the pool boundary is a much more difficult problem which involves the solution of coupled fluid flow and heat flow with a free boundary and is not considered in this paper. However, we can make the observation that, the more concentrated the current distribution, the smaller the width/depth ratio of the weld nugget should be. This effect is a plausible explanation for some experimental results by Willgoss (1978, private communication). His experiments produced stationary TIG welds in thick blocks of material. With argon as a shielding gas the width/depth ratio was around 2 (i.e. the pool boundary was roughly hemispherical). Adding some hydrogen to the shielding gas made the arc appear much more concentrated and deepened the pool considerably, producing a width/depth ratio as low as 1 in some cases. However, there was no indication of a 'keyhole' having formed in the pool surface. It is difficult to imagine a physical mechanism other than electromagnetic stirring which will produce a width/depth ratio lower than 2 in a thick specimen.

I would like to thank the referees for their constructive criticism of an earlier version of this paper. This paper is published with the permission of the Central Electricity Generating Board.

REFERENCES

ABRAMOWITZ, M. & STEGUN, I. A. 1964 *Handbook of Mathematical Functions.* Washington: National Bureau of Standards.

ANDREWS, J. G. & CRAINE, R. E. 1978 *J. Fluid Mech.* **84**, 281.

KUBLANOV, V. & EROKHIN, A. 1974 *Int. Inst. Weld Doc.* no. 212-318-74.

LANDAU, L. D. & LIFSHITZ, E. M. 1959 *Fluid Mechanics.* Pergamon.

LONGWORTH, D. 1975 In *Moving Boundary Problems in Heat Flow and Diffusion* (ed. J. R. Ockendon & W. R. Hodgkins). Clarendon.

MOORE, D. R., PECKOVER, R. S. & WEISS, N. O. 1973 *Comp. Phys. Comm.* **6**, 198.

ORZAG, S. A. & ISRAELI, M. 1974 *Ann. Rev. Fluid Mech.* **6**, 281.

QUIGLEY, M. B. C. 1977 *Weld & Metal Fab.* **45**, 619.

ROACHE, P. J. 1972 *Computational Fluid Dynamics.* Albuquerque: Hermosa.

ROSENTHAL, D. 1941 *Weld J. Res. Suppl.* **20**, S220.

SHERCLIFF, J. A. 1970 *J. Fluid Mech.* **40**, 241.

SOZOU, C. 1971 *J. Fluid Mech.* **46**, 25.

SOZOU, C. & PICKERING, W. M. 1976 *J. Fluid Mech.* **73**, 641.

SOZOU, C. & PICKERING, W. M. 1978 *Proc. Roy. Soc.* A **362**, 509.

WEIR, A. D. 1976 *J. Fluid Mech.* **75**, 49.

WOODS, R. A. & MILNER, D. R. 1971 *Weld J. Res. Suppl.* **50**, S163.